IEEE Access
Multidisciplinary | Rapid Review | Open Access Journal

Received July 21, 2019, accepted August 8, 2019, date of publication August 20, 2019, date of current version September 3, 2019.

Digital Object Identifier 10.1109/ACCESS.2019.2936400

High-Performance Robust Controller Design of Plug-In Hybrid Electric Vehicle for Frequency Regulation of Smart Grid Using Linear Matrix Inequality Approach

SAJAL KUMAR DAS[1], MIZANUR RAHMAN[1], SANJOY KUMAR PAUL[2], MANIZA ARMIN[1], PRIYO NATH ROY[3], AND NOROTTOM PAUL[4]

[1]Department of Mechatronics Engineering, Rajshahi University of Engineering & Technology, Rajshahi 6204, Bangladesh
[2]UTS Business School, University of Technology Sydney, Broadway, NSW 2007, Australia
[3]Department of Mechatronics Engineering, Khulna University of Engineering & Technology, Khulna 9203, Bangladesh
[4]Bangladesh Hi-Tech Park Authority (BHTPA), Information & Communication Technology Division, Dhaka 1207, Bangladesh

Corresponding author: Mizanur Rahman (mizan138027@gmail.com)

This work was supported and funded by the Bangabandhu Rajshahi Hi-Tech Park (Borendro Silicon City), Project under Bangladesh Hi-Tech Park Authority, Information and Communication Technology Division.

ABSTRACT This paper proposes a high-performance and robust linear quadratic regulator-proportional integral derivative (LQR-PID) controller for frequency regulation in a two-area interconnected smart grid with a population of plug-in hybrid electric vehicles. Controller robustness is achieved using a linear matrix inequality approach. The proposed control framework is tested in a simulated two-area interconnected smart grid integrated with plug-in hybrid electric vehicles under load disturbances and wind power fluctuations. The performance of the proposed controller is simulated using Matlab and compared with that of a conventional linear quadratic regulator controller. Simulation results show that the proposed controller provides reliable smart grid frequency control.

INDEX TERMS Smart grid, frequency control, linear matrix inequality.

I. INTRODUCTION

Electricity is essential to modern society. Accordingly, over-reliance on electrical energy generated from fossil fuels is a potential threat to energy security [1]. In addition, the consumption of fossil fuels produces greenhouse gas emissions that contribute to global warming. These problems can be mitigated if renewable energy sources (RESs) such as wind energy, hydro-power, and photovoltaic generation are used instead of fossil fuels. Compared to fossil fuel generation, RESs are clean, abundant, inexpensive and eco-friendly [2]. Of course, integration of RESs into traditional electricity grids is challenging, as traditional grid systems are weak, unreliable, inefficient, and transmit low-quality power. In addition, traditional grid systems use one-way links for the transmission, distribution, and control of electric power. Smart grids (SGs), on the other hand, are a viable way to cope with the challenges faced by traditional grids [3].

The associate editor coordinating the review of this article and approving it for publication was Engang Tian.

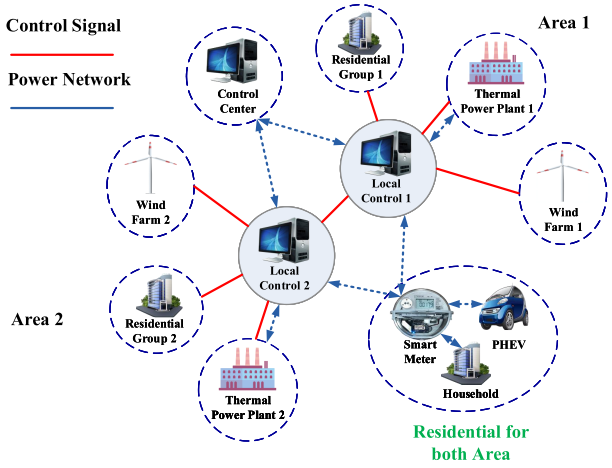

FIGURE 1. Schematic illustration of a smart grid system.

A two-area interconnected SG is shown in Fig. 1. Such grids require their components to be ''smart'', meaning that they have generation, transmission, metering, and protection

systems that can be adjusted automatically according to the requirements of the grid [4]. Such arrangements aim to reduce failure rates and improve reliability. A two-way interactive process is used in SGs for the transmission of power and information. To deal with uncertainty, SGs use self-adapting systems [5]. They aim to reduce reliance on fossil fuels and to improve the quality of power. Other advantages are that greenhouse gas emissions can be minimized and electricity consumers are given greater control over their consumption [6].

There are several challenges and constraints in the implementation of SGs, such as nonlinearity and stochasticity of practical systems [7], installing high-technology infrastructure, minimizing distribution losses, providing security, using renewable energy sources, and increasing customer awareness of SGs [8]. Renewable energy generation can require larger land areas than fossil fuel generation. Additionally, frequency fluctuations are more common, since the output power is not always as expected. Hence, uncertainty needs to be considered and compensated [9]. Changes in uncertainties can be caused by various circumstances, such as changes in available wind and sunlight, and other operational changes. These uncertainties bring about unexpected occurrences such as voltage variations and harmonic distortions which require the synchronization of generation sources with the grid [10].

Hybrid electric vehicles (HEVs) are a less-polluting alternative to present-day transportation systems [11]. These HEVs operate with little greenhouse gas emissions and noise pollution. An HEV consisting of an electric motor and a battery pack is clearly less polluting than a traditional vehicle [12]. However, the HEV concept is not completely flawless as it can involve battery degradation and high initial investment. An improved version of the HEV is the plug-in hybrid electric vehicle (PHEV), which can be charged at any available outlet, travel greater distances, and even reduce frequency fluctuations in SGs [13]. A PHEV can act as an energy storage device for which charging and discharging can be bidirectional or unidirectional. The bidirectional mode has some advantages: it can aid active power, control reactive power, and assist the integration of RESs [14]. While the output obtained from RESs is sporadic and dependent on meteorological conditions, PHEVs can store energy to mitigate this problem. At the same time, PHEVs can attenuate power fluctuations in SGs as they have a user-controlled frequency regulation option [15].

These PHEVs can be regarded as distributed energy storage systems. They can provide faster supplementary service to a grid. The storage capacity of PHEVs has been used in electric grids for many years [16]. The vehicle-to-grid (V2G) concept has become popular in recent years. It enables energy to be stored and supplied to the grid. A V2G system can respond more rapidly to grid fluctuations than generators and turbines, thereby improving grid efficiency, reliability, and performance. A V2G system can also help consumers [17], who can earn revenue by storing electricity. The most important task of PHEVs is frequency regulation. When there is a mismatch between generation and demand, the grid frequency deviates from its nominal value. Hence, a control framework is required to maintain the frequency deviation within a nominal range. However, the time constant of PHEVs hampers the frequency deviation correction. The battery pack of PHEVs can be considered as a distributed energy storage system. Moreover, the transient response of a PHEV is way faster than that of a generator, which makes it more compatible with the grid. However, there are some drawbacks to PHEVs such as battery degradation and the cost of new infrastructure [18].

A number of decentralized load frequency controllers have been proposed in the literature, which have several functions: 1) ensuring zero steady-state errors for frequency fluctuations, 2) controlling unscheduled tie-line power deviation, 3) providing robust performance against sudden load changes, 4) compensating for transient variations in tie-line power, and 5) maintaining a prescribed overshoot and settling time. The classical control technique includes several classical controllers. A control framework is used in a governor to regulate frequency deviations. In [19], Nyquist and Bode plot have been proposed for frequency regulation of power system. Their analysis is based on gain and phase margins. A dual-mode proportional integral (PI) controller for frequency regulation was proposed in [20]. The decentralized PI control technique has been described in [21]. In [22], a predictive controller was modeled for SG frequency regulation. The controller has a unique feature that predicts future output and it demonstrated robust performance against load perturbations. It is also suitable for nonlinear systems. Integral derivative (ID) controllers were used for load frequency control problems in [23]. The chaotic optimization technique was used for tuning the PID parameter in [24]. Study [25] compared the use of a PI plus a double derivative controller with an integral plus double derivative approach to frequency stabilization. There are several disadvantages to these classical control methods. These controllers show poor parameter tuning performance and do not perform well in mitigating system parameter variations and uncertainty. Cyber-attack is another risk to classical controllers.

The optimal control framework has been proposed for frequency regulation in power systems. This method provides solutions for multivariate systems for designing the control signal and is applicable when the state variables are observable. It is a good tracking control technique. This type of controller is optimal when the system model is based on a set of differential equations. The control framework design process is very easy. The cost of the controller is a quadratic function. The design of the controller is based on minimization of the cost function. The linear quadratic regulator (LQR) has been proposed for frequency control in interconnected power systems [26] and is a linear-quadratic regulator associated with a Kalman filter. This filter is used to estimate the incomplete state information with added a Gaussian white noise. It has the ability to reduce the estimated error when Gaussian random noise is considered. This controller is able to predict

the future steps of the system to be controlled [27]. There are several disadvantages to the optimal control method. For example, it requires the determination of the dynamic state of the system. Cyber-attack should also be considered when designing the controller. Parameter uncertainty is another requirement of the design, while a limitation of this control method is that it requires the design of a dynamic observer.

Adaptive control schemes have also been proposed for frequency stabilization [28]. This control technique is effective if the operating point varies with time. Hence, it requires updating of the parameters. Adaptive control can be divided into self-tuning control (STC) and model reference control. In [29], STC was designed for frequency stabilization power system. This control method was also used for the Hungarian power system. In [30], the combination of a PID controller and an adaptive controller was reported for frequency regulation. An adaptive neuro-fuzzy model was used for frequency stabilization in [31]. Adaptive fuzzy gain scheduling was used for load frequency control in [32]. The adaptive control technique has several disadvantages. The control method is complex and requires a standard model, making it difficult to implement in real time.

Riccati equation-based robust controllers were designed for frequency stabilization in [33] and [34]. These controllers have robust performance in uncertain scenarios. A combination of robust and adaptive control schemes was modeled in [35]. In this method, the robust controller deals with small uncertainties and the adaptive controller takes care of large uncertainties. A linear matrix inequality (LMI) based control technique was designed in [36]. This method ensures robust performance in uncertain scenarios and parameter variations. A combination of the Riccati equation and Lyapunov stability theory was proposed for frequency stabilization of power system in [33] and have several benefits. It can handle parameter variations and has disturbance rejection capability. However, its drawbacks are that it requires proper knowledge of the system and it performs poorly against cyber-attack and unknown variable input.

Intelligent control approaches have been proposed for SG frequency regulation, artificial neural networks (ANNs), genetic algorithms (GAs) and fuzzy logic. These methods are low cost than traditional control schemes and can be implemented easily in real time. The control techniques show robust performance against uncertainties, non-linearities, and disturbances. An ANN was proposed for load frequency control in [37]. The main drawback of this control technique is its high training time. The performance of ANNs can also deviate due to poor selection of weighting matrices. Fuzzy logic has been used to compensate for SG frequency fluctuations [38]. The controller can be designed based on human concepts and opinions about a system. The limitation of the controller is the tuning of the membership functions. A fuzzy PI control scheme was reported in [39]. The disadvantage of this controller is its poor transient response. A GA-based control framework for a multi-area interconnected SG was modeled in [40]. The technique can be applied to improve the dynamic performance of the system; however, the controller requires good heuristic knowledge. A particle swarm optimization (PSO) algorithm was developed for frequency regulation of a multi-area tie-in power system in [41]. The limitation of the algorithm is its relatively slow convergence.

In this paper, we propose a novel, robust, LQR-PID framework for frequency stabilization of interconnected SGs. Though conventional controllers provide good performance, they cannot ensure robust stability against system uncertainties. The contribution of this paper is the design of a novel control approach to frequency stabilization in an interconnected power system. This control approach is based on a convex optimization technique involving LMI, which can be solved in polynomial time. The goal of designing the proposed controller is to achieve robust performance against various system uncertainties such as variations in system parameters, wind power generation, and load. This proposed control technique ensures robust stability within an uncertain polytypic set. Moreover, it can be implemented online and has a large bandwidth, large gain, and phase margin. Although the proposed controller was designed for frequency stabilization of a two-area interconnected SG, it can also be implemented in a number of applications such as nanopositioning control [42], robotics control [43], navigation control [44], smart actuator control [45], hard disk drive control [46], and others where robust tracking of a reference is important. The performance of the controller was simulated using a Matlab environment. The simulation results were analyzed for a two-area interconnected SG populated with PHEVs. The simulation results show that the proposed controller provides robust performance against various uncertainties. It also provides a superior frequency control effect in comparison with LQR controllers.

The remainder of this paper is organized as follows. Section II represents the modeling of the SG. The control framework is described in Section III. Section IV provides a performance evaluation, while Section V concludes the paper.

II. SYSTEM MODELLING

A linearized model of a two-area tie-in SG system [49], [50], [47] is shown in Fig. 2, which was used for the analysis of the SG. Each area has a wind farm (WF), governor-turbine, controller, PHEVs, and load. The local control center can send control signals to the PHEVs via smart meters. A tie-line is used to exchange power between two adjacent areas. Frequency deviation occurs due to generation-load imbalances and tie line power flow. The governor can sense frequency deviations and adjusts the valve position to keep them within a nominal value. The governor and turbine comprise the primary frequency control of the generating unit. This primary control is unable to restore frequency deviations and a secondary control system, like load frequency controller and PHEVs, is necessary to adjust the generation-load imbalance or tie line power flow. In Fig. 2, the load is modeled by a 1^{st}-order transfer function with inertia constant D and damping coefficient M. The PHEVs, wind power and load

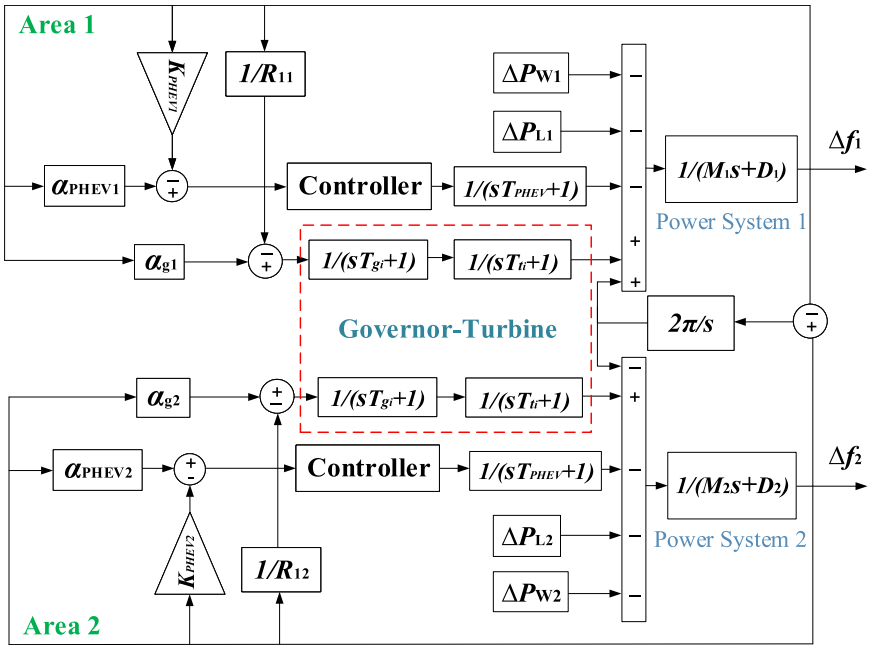

FIGURE 2. Linearized model of a two-area interconnected smart grid.

are modeled by $\alpha_{PHEV,i}$, $\Delta P_{wind,i}$ and ΔL_i, where i=1,2,..,N, respectively. The system parameters and data for the two-area power system are given in Table 1. The turbine dynamics can be expressed as:

$$\Delta \dot{P}_{mk,i} = -\frac{1}{T_{Tk,i}}\Delta P_{mk,i} + \frac{1}{T_{Tk,i}}\Delta P_{Gk,i} \tag{1}$$

where $\Delta P_{mk,i}$, $\Delta P_{Gk,i}$ and $T_{Tk,i}$ are the generator mechanical power deviation, change in output power, and turbine time constant in area i, respectively. The governor dynamics are expressed as:

$$\Delta \dot{P}_{Gk,i} = -\frac{1}{R_{ki}T_{Gk,i}}\Delta f_i - \frac{1}{T_{Gk,i}}\Delta P_{Gk,i} + \frac{1}{T_{Gk,i}}\Delta P_{L,i} \tag{2}$$

Here, Δf_i, $\Delta P_{L,i}$, $T_{Gk,i}$, and R_{ki} are the frequency deviation, load disturbance, governor time constant, and speed droop coefficient in area i, respectively. The droop characteristic is the ratio of frequency change to change in output-generated power. The droop characteristic can be expressed as:

$$R_{ik} = \frac{\Delta f_i}{\Delta P_{gki}} \tag{3}$$

Here, ΔP_{gki} and R_{ki} are the change in output power and droop characteristic of k^{th} generating unit in area i, respectively.

The governor and turbine model of the k^{th} generating unit in area i can be expressed in terms of $M_{ki}(s)$ as:

$$M_{ki}(s) = \frac{1}{1+T_{Gk,i}(s)}\frac{1}{1+T_{Tk,i}(s)} \tag{4}$$

In a multi-area power system, the generation-load relationship can be modeled as follows:

$$\Delta P_{Net,i} = 2M_i(d\Delta f_i(t)/dt) + D_i\Delta f_i(t) \tag{5}$$

TABLE 1. System parameters values for frequency simulation model [47], [48].

Parameters	Area 1	Area 2
$T_{Tk,i}$(s)	0.401	0.443
$T_{Gk,i}$(s)	0.085	0.067
R_{ik}(Hz/pu)	3.02	2.675
α_i(pu/Hz)	1.0236	1.2857
$M_{(i)}$	0.2533	0.2839
D_i (pu.MW/Hz)	0.0450	0.0460
$T_{PHEV,i}$	1.00	1.00

Here, $\Delta P_{Net,i} = \Delta P_{mk,i} - \Delta P_{L,i}$ is responsible for the frequency deviation Δf_i in area i.

The tie-line power $\Delta P_{tie,i}$ is the summation of the real power that comes from a control area i. The power equals the sum of all out-flowing line power, $P_{tie,ij}$ in the lines connecting area i with neighbouring area j, i.e.

$$\Delta P_{tie,i} = \sum P_{tie,ij} \tag{6}$$

The simulations can be applied to all lines j that terminate in area i. By letting the line loss equal zero, the tie-line power can be written as follows:

$$\Delta P_{tie,ij} = \frac{|V_i||V_j|}{X_{ij}P_{ri}}sin(\delta_i - \delta_j) \tag{7}$$

where X_{ij} is the reactance of the tie-line connecting areas i and j. The parameters V_i and V_j are the bus voltages of the line. When the phase angles deviate from their nominal values δ_i^0 and δ_j^0 by the amounts of $\Delta\delta_i$ and $\Delta\delta_j$, respectively, the incremental power $\Delta P_{tie,ij}$ over the line can be defined

as follows:

$$\Delta P_{tie,i} = \frac{\Delta P_{tie,i}}{\partial(\delta_i - \delta_j)}(\Delta\delta_i - \Delta\delta_j) \tag{8}$$

Also:

$$\frac{\Delta P_{tie,i}}{\partial(\delta_i - \delta_j)} = P_{tie,max,ij}cos(\delta_i^0 - \delta_j^0) \tag{9}$$

The phase angles are related to the frequency deviation as follows:

$$\Delta\delta_i = 2\Pi \int \Delta f_i dt \tag{10}$$

From the above equations, we get:

$$\Delta P_{tie,ij} = 2\Pi \frac{|V_i||V_j|}{X_{ij}P_{ri}} cos(\delta_i^0 - \delta_j^0) \tag{11}$$

$$or, \Delta P_{tie,ij} = T_{ij}[\int \Delta f_i dt - \int \Delta f_j dt] \tag{12}$$

Here, $T_{ij} = 2\Pi \frac{|V_i||V_j|}{X_{ij}P_{ri}} cos(\delta_i^0 - \delta_j^0)$, where $\Delta P_{tie,i}$ is the change in tie line power in area i. The parameter T_{ij} is the synchronizing torque coefficient between areas i and j. Δf_i and Δf_j are the frequency deviations between the areas i and j, respectively.

The total power flow in each area can be represented as:

$$\Delta P_{Net,i} = \Delta P_{m,i} - \Delta P_{tie.i} - \Delta P_{L.i} - \Delta P_{PHEVs,i} \tag{13}$$

Here, $\Delta P_{Net,i}$, $\Delta P_{L,i}$, and $\Delta P_{PHEVs,i}$ are the total generation-load imbalance, load disturbance, and total output power from all PHEVs in area i. By combining (1), (2) and (5), the frequency deviation in each area can be represented as follows:

$$\Delta f_i(s) = \frac{\Delta P_{m.i} - \Delta P_{tie,i} - \Delta P_{L,i} - \Delta P_{PHEVs,i}}{2M_{is} + D_i} \tag{14}$$

From equation (6), we can see that the power from all PHEVs in each area can compensate for the load disturbance in the grid and reduce frequency fluctuations. The PHEVs participating for frequency regulation in SG. Assuming the state of charge (SoC) of each PHEVs has been considered to 0.90. Fig. 3 shows the relationship between PHEV power and frequency fluctuation. Abbreviation V1G denotes the one-way charging of vehicles from the grid, while V2G denotes two-way charging/discharging (from vehicle to grid or grid to vehicle). The power of each PHEV is regulated by the droop characteristic. The power of PHEVs can be added to the grid with consideration of frequency fluctuations as follows:

$$\underline{P}_{V2G} = \begin{cases} \underline{\mathcal{K}}_{V2G}.\Delta f & |\underline{\mathcal{K}}_{V2G}.\Delta f| \le \underline{P}_{max} \\ \underline{P}_{max}, & \underline{\mathcal{K}}_{V2G}.\Delta f > \underline{P}_{max} \\ -\underline{P}_{max}, & \underline{\mathcal{K}}_{V2G}.\Delta f < -\underline{P}_{max} \end{cases} \tag{15}$$

Here, $\underline{P}_{max}$ represents the maximum power of V2G, while $\underline{\mathcal{K}}_{V2G}$ is the vehicle to grid gain. The gain can be achieved from the maximum gain of PHEVs: $\mathcal{K}_{max}$. The SoC can be managed in a specific range. The SoC and $\underline{\mathcal{K}}_{V2G}$ are defined as:

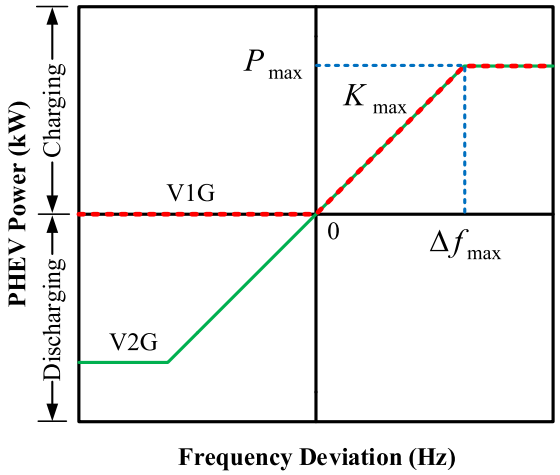

FIGURE 3. Relationship between PHEV power and frequency deviation.

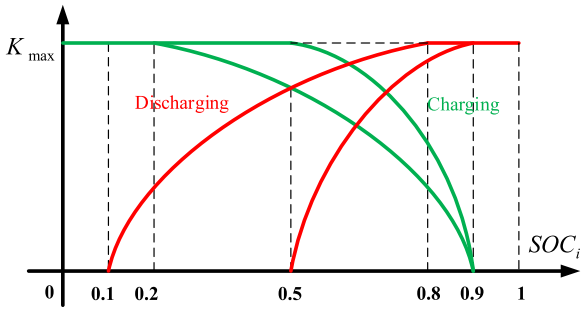

FIGURE 4. Relationship between battery gain and state of charge.

$$\underline{\mathcal{K}}_{V2G} = \underline{\mathcal{K}}_{max}[1 - (\frac{SoC - SoC_{low(high)}}{SoC_{max(min)} - SoC_{low(high)}})]^n \tag{16}$$

Here, SoC_{low} and SoC_{high} represent the low and high state of charge, respectively. The parameter n is the specification of the battery SoC. Parameter $\mathcal{K}_{max}$ can be adjusted by taking account of PHEVs and the deviation in SoC. The impacts of SoC and PHEVs are described in [51] and [52]. Fig. 4 shows the relationship between battery gain and SoC, showing that $SoC_{min} = 0.1$, $SoC_{low} = 0.2$, $SoC_{high} = 0.8$, $SoC_{max} = 0.9$, and n=2. The SoC is maintained in a range of 0.5. Similarly, the SoC is kept balance at 0.7 by setting $SoC_{min} = 0.5$, $SoC_{low} = 0.5$, $SoC_{high} = 0.9$, and $SoC_{max} = 0.9$. Hence, the various SoC terms make various SoC balances. The parameter $\underline{\mathcal{K}}_{V2G}$ is calculated from (16) and can be used in (15). The positive and negative frequencies are used to calculate the PHEV charging and discharging rates. When the frequency becomes negative, the discharging power can be calculated from (15). The positive frequency is used to determine the charging power with a gain of $\underline{\mathcal{K}}_{V2G}$. The relationship between charging-discharging and SoC can be modeled by a quadratic equation. The total power and frequency deviation follow a non-linear equation. The frequency deviation can be calculated according to Equation (16). When

the SoC is approximately full, charging cannot be recommended, so that overcharging is avoided. The PHEVs are used to stabilize the frequency by considering discharge power in relation to the SoC limitation. The parameter $\underline{\mathcal{K}}_{V2G}$ will increase with increase in SoC. When the PHEVs are engaged for frequency regulation by charging power, then $\underline{\mathcal{K}}_{V2G}$ will decline with the addition of SoC. If the SoC is not within an acceptable range, then $\underline{\mathcal{K}}_{V2G} = 0$ and the PHEVs are not engaged in frequency regulation. Balance control is also used to compensate the frequency fluctuation. Each PHEV has an initial SoC which is used to add the level of SoC for time-driven system. Hence, frequency fluctuation can be improved by using PHEVs. The gain parameter $\underline{\mathcal{K}}_{V2G}$ may be used to enhance the frequency deviation, as introduced in [53].

A closed-loop control framework for PHEVs is shown in Fig. 2. A state space model of the PHEV control framework is defined as follows:

$$\begin{aligned} \dot{x}(t) &= Ax(t) + Bu(t) \\ y &= Cx(t) \end{aligned} \tag{17}$$

$$A = \begin{bmatrix} -1/T_{PHEV} & 0 \\ -1/M & -D/M \end{bmatrix}; \quad B = \begin{bmatrix} 1/T_{PHEV} \\ 0 \end{bmatrix};$$
$$C = \begin{bmatrix} 0 & 1 \end{bmatrix}; D = \begin{bmatrix} 0 \end{bmatrix}; \tag{18}$$

Here, T_{PHEV}, D, and M are the PHEV time constant and the damping and inertia coefficients, respectively.

III. CONTROLLER DESIGN

A. LQR CONTROLLER

From the LTI system in (17), the objective function of the system is to find the control input vector $u[.]$ that minimizes the cost function:

$$\mathcal{J}_{lqr} = \int_0^\infty (\underline{x}^T Q \underline{x} + u^T R u) dt \tag{19}$$

for any elementary state vector $\underline{x}(0)$ in which Q is defined as a weighted matrix of the state and R is defined as a control input weighted matrix, such that $Q = Q^T \geq 0$ and $R = R^T > 0$, respectively. Assuming (A, B) and $(Q)^{\frac{1}{2}}$ are controllable and observable, then the control input $u[.]$ minimizing $\mathcal{J}_{lqr}$ is defined as a state feedback gain:

$$u = -\mathcal{K}\underline{x} \tag{20}$$

where $\mathcal{K} = -R^{-1}B^T\mathcal{P}$ and $\mathcal{P} = \mathcal{P}^T > 0$ is the solution of the algebraic Riccati equation (ARE)

$$A^T\mathcal{P} + \mathcal{P}A - \mathcal{P}BR^{-1}B^T\mathcal{P} + Q = 0 \tag{21}$$

and the minimum cost function is defined as:

$$\mathcal{J}_{min}(u) = \int_0^\infty (\underline{x}^T(0) Q \underline{x} + u^T R u) dt \tag{22}$$

The aforementioned approach concludes that the LQR solution depends on the solution of $\mathcal{P}$ in (21).

Now, consider an uncertain second order system:

$$\mathrm{T}(s) = \frac{a}{s^2 + b_1 s + b_2} \tag{23}$$

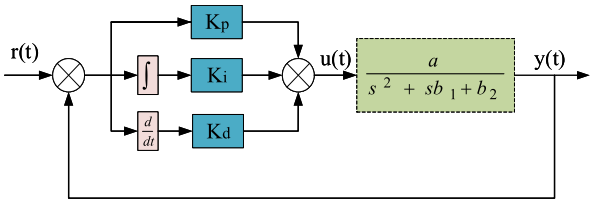

FIGURE 5. Block diagram of the closed-loop system.

where the parameters vary in the intervals:

$$b_1 \epsilon [\underline{b_1}, \overline{b_1}], b_2 \epsilon [\underline{b_2}, \overline{b_2}]; a \epsilon [\underline{a}, \overline{a}] \tag{24}$$

From the closed-loop system in Fig. 5, the states are:

$$\begin{aligned} \underline{x}_1 &= e(s) \\ \underline{x}_2 &= \frac{e(s)}{s} \\ \underline{x}_3 &= se(s) \end{aligned} \tag{25}$$

$$\frac{Y(s)}{U(s)} = \frac{a}{s^2 + b_1 s + b_2} = \frac{E(s)}{U(s)} \tag{26}$$

$$E(s)(s^2 + b_1 s + b_2) = bU(s) \tag{27}$$

Solving the equations in (25) and (27), the state-space model is given as follows:

$$\begin{bmatrix} \dot{\underline{x}}_1 \\ \dot{\underline{x}}_2 \\ \dot{\underline{x}}_3 \end{bmatrix} = \begin{bmatrix} 0 & 1 & 0 \\ 0 & 0 & 1 \\ 0 & -b_2 & -b_1 \end{bmatrix} \begin{bmatrix} \underline{x}_1 \\ \underline{x}_2 \\ \underline{x}_3 \end{bmatrix} + \begin{bmatrix} 0 \\ 0 \\ a \end{bmatrix} U \tag{28}$$

From Equation (28), the closed-loop system matrices are

$$A = \begin{bmatrix} 0 & 1 & 0 \\ 0 & 0 & 1 \\ 0 & -b_2 & -b_1 \end{bmatrix}, \quad B = \begin{bmatrix} 0 \\ 0 \\ a \end{bmatrix} \tag{29}$$

Hence, the state feedback gain of the above system can be determined as follows:

$$\mathcal{K} = -R^{-1}B^T\mathcal{P} = -R^{-1}\begin{bmatrix} 0 & 0 & a \end{bmatrix} \begin{bmatrix} \mathcal{P}_{11} & \mathcal{P}_{12} & \mathcal{P}_{13} \\ \mathcal{P}_{21} & \mathcal{P}_{22} & \mathcal{P}_{23} \\ \mathcal{P}_{31} & \mathcal{P}_{32} & \mathcal{P}_{33} \end{bmatrix}$$
$$= -R^{-1}a \begin{bmatrix} \mathcal{P}_{13} & \mathcal{P}_{23} & \mathcal{P}_{33} \end{bmatrix} = -[\mathcal{K}_p \; \mathcal{K}_i \; \mathcal{K}_d] \tag{30}$$

Prior to the design of the robust PID controller, the following section is needed to understand how the LQR problem is converted into LMIs which provides the basic lyapunov function. The quadratic lyapunov function is the solution of the linear system which ensures the internal stability and provides the desired performance [54].

B. STABILITY OF AN LTI SYSTEM

In both practical and simulation analyses of a dynamical system, stability checking is very important. This system stability analysis role is carried out according to the fields of systems theory and engineering. A stability checking method for a linear system was proposed in [55]. Additionally, the stability of a non-linear system can be investigated using linear methods such as binary distillation and pH neutralization. The necessary stability condition of the closed-loop system in (28) is carried out according to the Lyapunov stability theorem.

Lyapunov Stability Criterion [55]: The Lyapunov technique is a well-known method of stability analysis. The main concept behind the Lyapunov technique is to determine the positive definite function. The time derivative of the function is a negative definite function. Consider a transfer function matrix $R(s)$ that has a minimal state-space realization (A, B, C, D), such that:

$$\dot{\underline{x}}(t) = A\underline{x}(t) + Bu(t) \tag{31}$$

$$y(t) = C\underline{x}(t) + Du(t) \tag{32}$$

Here, $\underline{x}[.]$ and $u[.]$ are the state vector and input vector of the system, respectfully. The system in (31) is asymptotically stable if it satisfies the following Lyapunov function:

$$A^T\mathcal{P} + \mathcal{P}A < 0 \tag{33}$$

such that $\mathcal{P} > 0$.
where, $\mathcal{P}$ a symmetric positive definite matrix.

Lemma 1 [54]: The schur compliments of the following inequality:

$$\begin{bmatrix} V(x) & S(x) \\ S^T(x) & \mathcal{P}(x) \end{bmatrix} > 0,$$

is equivalent to

$$\mathcal{P}(x) > 0, \quad V(x) - S(x)\mathcal{P}^{-1}S^T(x) > 0$$
$$V(x) > 0, \quad \mathcal{P}(x) - S(x)V^{-1}(x)S^T(x) > 0$$

where $V(x) = V^T(x), \mathcal{P}(x) = \mathcal{P}^T(x)$, and $S(x)$ affinely depend on x.

Lemma 2 [56]: Assuming matrices A, $\mathcal{W} = \mathcal{W}^T > 0$, and $Q = Q^T$ are defined. If the ARE
$\mathcal{P}\mathcal{W}\mathcal{P} = \mathcal{P}A + A^T\mathcal{P} + Q$
has a real positive symmetric matrix $\mathcal{P}$, then for any $0 < \mathcal{W}_1 \leq \mathcal{W}$ and $Q_1 \geq Q$, the equation

$$\mathcal{P}_1\mathcal{W}_1\mathcal{P}_1 = \mathcal{P}_1A + A^T\mathcal{P}_1 + Q_1$$

has a real positive symmetric matrix $\mathcal{P}_1 \geq \mathcal{P}$.

C. LMI LQR-PID CONTROLLER DESIGN

The state feedback gain in (30) can be designed according to a linear matrix inequality (LMI) approach [57]. In this section, the gain of the PID controller is designed based on the LMI-LQR framework. For any LTI system according to (28), the LQR optimization problem can be expressed as:

$$\min_{\hat{\mathcal{P}},Y} x^T(0)\hat{\mathcal{P}}^{-1}x(0) \tag{34}$$

subject to

$$\begin{bmatrix} A\hat{\mathcal{P}} + \hat{\mathcal{P}}A^T + BY + Y^TB^T & \hat{\mathcal{P}} & Y^T \\ \hat{\mathcal{P}} & -Q^{-1} & 0 \\ Y & 0 & -R^{-1} \end{bmatrix} \leq 0, \ \hat{\mathcal{P}} > 0 \tag{35}$$

where $Y = \mathcal{K}\hat{\mathcal{P}}$ and $\hat{\mathcal{P}} = \mathcal{P}^{-1}$.

Proof: Consider a transfer function matrix with a minimal state space representation T(A, B, C, D) where (A, B) and (A, C) are controllable and observable, respectively. Now, the minimum cost function $\mathcal{J}_{min}$, where Q and R are symmetric positive definite matrices, of T(s) is defined as

$$\mathcal{J}_{min} = \int_0^\infty (x^TQx + u^TRu)dt \tag{36}$$

Then the following inequalities are analogous:

(i) $A^T\mathcal{P} + \mathcal{P}A - \mathcal{P}BR^{-1}B^T\mathcal{P} + Q = 0$ such that $\mathcal{P} = \mathcal{P}^T > 0$

(ii) The feasibility function of the inequality is

$$A^T\mathcal{P} + \mathcal{P}A + Q + \mathcal{K}^TB^T\mathcal{P} + \mathcal{P}BK + K^TRK \leq 0 \tag{37}$$

where, $\mathcal{P}$ and $\mathcal{K}$ are variable.

(iii) The feasibility of the LMI is

$$\begin{bmatrix} A\hat{\mathcal{P}} + \hat{\mathcal{P}}A^T + BY + Y^TB^T & \hat{\mathcal{P}} & Y^T \\ \hat{\mathcal{P}} & -Q^{-1} & 0 \\ Y & 0 & -R^{-1} \end{bmatrix} \leq 0$$

(iv) $\mathcal{M} = \begin{bmatrix} A & -BR^{-1}B^T \\ -Q & -A^T \end{bmatrix}$

Where, $\mathcal{M}$ is the Hamiltonian matrix.

Hardly speaking, there is no need to prove that (i) and (iv) are equivalent (from linear regulator theory). However, for (ii) and (iii), assume that $\hat{\mathcal{P}} = \mathcal{P}^{-1}$ and $Y = K\hat{\mathcal{P}}$. Multiplying both sides of (37) by $\hat{\mathcal{P}}$, we get

$$A^T\hat{\mathcal{P}} + \hat{\mathcal{P}}A + \hat{\mathcal{P}}Q\hat{\mathcal{P}} + \hat{\mathcal{P}}K^TB^T + BK\hat{\mathcal{P}} + \hat{\mathcal{P}}K^TRK\hat{\mathcal{P}} \leq 0$$
$$= A^T\hat{\mathcal{P}} + \hat{\mathcal{P}}A + \hat{\mathcal{P}}QP + Y^TB^T + BY + Y^TRY \leq 0 \tag{38}$$

Now, applying schur complement (lemma 1), it is found that (ii) and (iii) are equivalent. However, from lemma 2, there exists a symmetric matrix $\mathcal{P}_1 = \mathcal{P}_1^T > 0$ such that the following LMI

$$A^T\mathcal{P}_1 + A\mathcal{P}_1 + Q - \mathcal{P}_1BR^{-1}B^T\mathcal{P}_1 \leq 0 \tag{39}$$

is feasible. By choosing $K = -R^{-1}B^T\mathcal{P}_1$, we get

$$A^T\mathcal{P}_1 + A\mathcal{P}_1 + Q + K^TB^T\mathcal{P}_1 + \mathcal{P}_1BK + K^TRK \leq 0$$
$$= A^T\mathcal{P}_1 + A\mathcal{P}_1 + Q - \mathcal{P}_1BR^{-1}B^T\mathcal{P}_1 \leq 0$$

which implies (ii). This concludes the proof.

However, (34) can also be rewritten as:

$$x^T(0)\hat{\mathcal{P}}^{-1}x(0) \leq \gamma \tag{40}$$

where γ defines the upper bounded value. Using the lemma 1, Equation (40) can be expressed as:

$$\begin{bmatrix} \gamma & x^T(0) \\ x^T(0) & \hat{\mathcal{P}} \end{bmatrix} \leq 0, \quad \hat{\mathcal{P}} > 0 \tag{41}$$

So, the state feedback gain in (30) can be obtained from the LMIs in (34) and (35), and is defined as:

$$\mathcal{K} = Y\mathcal{P}^{-1} = [\mathcal{K}_p \ \ \mathcal{K}_i \ \ \mathcal{K}_d] \tag{42}$$

For any practical system, the system matrices $[A,\ B]$ are uncertain. Let, $[A,\ B] \epsilon\ \Omega$, where Ω is a polytopic set with:

$$\Omega = Cov\{[A_1, B_1], [A_2, B_2], [A_3, B_3], \ldots, [A_{N_m}, B_{N_m}]\} \quad (43)$$

if, and only if

$$[A, B] = \sum_{i=1}^{N_m} w_i(x, u)[A_i, B_i] \quad (44)$$

where N_m represents multiple model numbers and $w_i \epsilon\ [0\ 1]$ refers to the weighting function satisfying:

$$\sum_{i=1}^{N_m} (x, u) = 1, \quad \mho(x, u) \epsilon\ R^{N_x} \times R^{N_u}$$

In (29) and (42), there are three uncertain parameters and, in (43), Ω is reduced to:

$$\Omega = Cov\{[A_1, B_1], [A_2, B_2], [A_3, B_3], \ldots, [A_8, B_8]\} \quad (45)$$

Here, the PID controller gain $\mathcal{K}$ holds all the uncertain parameters defined in (42). The vertex matrices $[A_i, B_i]$ are the permutation of the maxima and minima of the system matrices in (24).

D. PARAMETER ESTIMATION AND STABILITY TEST

The formulation of the closed-loop system is presented in this section and its robustness is evaluated. From the state-space representation in (17) and (17), the controlled system G(s) is a second-order system, as follows:

$$\frac{-1}{s^2 M T_{PHEV} + (T_{PHEV} D + M)s + D} \quad (46)$$

By comparing the above system with the uncertain second-order system in (23), we can depict the state-space model of the closed-loop system as:

$$\dot{\underline{x}} = \begin{bmatrix} 0 & 1 & 0 \\ 0 & 0 & 1 \\ 0 & \dfrac{D}{-MT_{PHEV}} & -\dfrac{M + DT_{PHEV}}{MT_{PHEV}} \end{bmatrix} \underline{x} + \begin{bmatrix} 0 & 0 & \dfrac{-1}{MT_{PHEV}} \end{bmatrix}^T u \quad (47)$$

Now, to formulate the state-feedback gain $\mathcal{K}$ for the proposed PID controller from (34) and (35), we have:

$$\mathcal{P} = \begin{bmatrix} 0.7718 & -0.6972 & 0.0268 \\ -0.6972 & 1.4233 & -1.8958 \\ -0.0268 & -1.8958 & 6.7422 \end{bmatrix} \quad (48)$$

$$Y = \begin{bmatrix} 0.5068 & -0.4374 & -10.7968 \end{bmatrix} \quad (49)$$

Therefore, the PID gain in the vector form is calculated as:

$$\mathcal{K} = \begin{bmatrix} \mathcal{K}_P & \mathcal{K}_i & \mathcal{K}_D \end{bmatrix} = Y\mathcal{P}^{-1} = \begin{bmatrix} 9.0132 & 10.8826 & 4.625 \end{bmatrix} \quad (50)$$

which ensures the robust stability of the closed-loop system within the polytopic set.

However, the closed-loop system stability is checked using the Lyapunov criterion. From the LMI in (33), $\mathcal{P}$ is established as:

$$\mathcal{P} = 1 \times 10^4 \times \begin{bmatrix} 0.0083 & 0.0997 & 0.0915 \\ 0.0997 & 4.0401 & 3.1015 \\ 0.0915 & 3.1015 & 6.2625 \end{bmatrix} \quad (51)$$

where all the eigenvalues are positive. Therefore, according to the Lyapunov criterion, the closed-loop system in (47) is asymptotically stable.

IV. PERFORMANCE EVALUATION

This section evaluates the performance of the proposed controller and compares it with that of a conventional LQR controller. An optimal controller, namely, a linear quadratic regulator (LQR) and state feedback controller (such as an LMI LQR-PID controller) is designed in this paper. The optimal controller minimizes the cost function while the state feedback controller minimizes the state feedback gain. The SG system was simulated using the Matlab environment.

Fig. 6(a) presents the time-domain response of the plant. The open loop response is the undesirable component of the response. The closed-loop time response of the LQR controller can show the tracking performance. The LMI LQR-PID shows higher performance compared to the LQR controller. It also eliminates steady-state errors. Fig. 6(b) shows the frequency domain response. The open loop resonance frequency is about 30 dB; while in a closed loop, it is close to 0 dB line. The LMI LQR-PID also ensures high gain and a high phase margin in comparison with the LQR controller.

The grid used in this evaluation is considered to be small. The power rating of each generator is 1 MW. The parameter values of the system will be fixed and disturbance will not be considered. A load disturbance of 0.05 pu in 0.1 seconds will be considered for both areas. A Matlab function is used to create the basic SoC of each vehicle. The initial SoC values range from 0.1 to 1. By neglecting losses, the efficiency is considered to be 100%. The robust performance of the controller is verified against several conditions, such as load changes, variable wind power and a large population of PHEVs. The parameter values shown in Table 1 are used to simulate the system. Frequency fluctuations and tie-line power variations are analyzed considering the following cases: 1) a traditional model, 2) an adjusted model an LQR controller, and 3) The proposed control method with PHEVs. Details of the simulation results for two-area tie-in SG are given below:

A. FREQUENCY DEVIATION PERFORMANCE ANALYSIS

Fig. 7(a) and (b) show the frequency deviations for Areas 1 and 2 for the interconnected SG, which has 500 and 100 PHEVs in Areas 1 and 2, respectively. From these results, the conventional model appears to have the largest frequency deviation. The closed-loop response with the LQR controller reduces the frequency deviation, although it contains

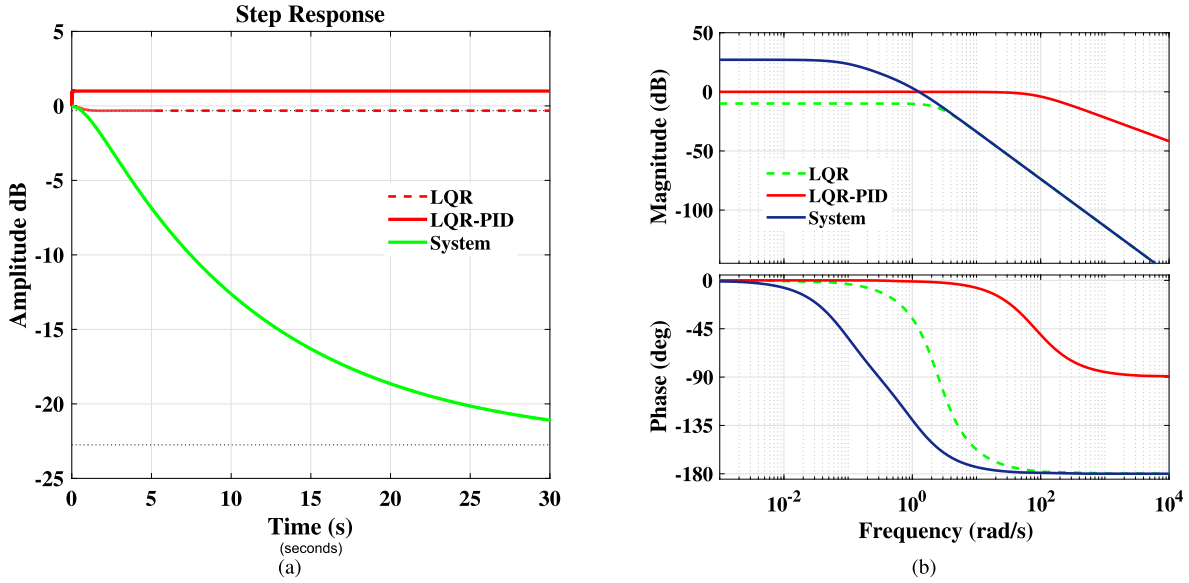

FIGURE 6. (a) Comparison of step response: The solid green line (-) represents open-loop response for the system. The red dashed (- -) line and red solid (-) line present the closed-loop response of LQR and LMI LQR-PID controller respectively. (b) Comparison of the Bode diagram in open and closed-loop using the proposed controller and LQR controller.

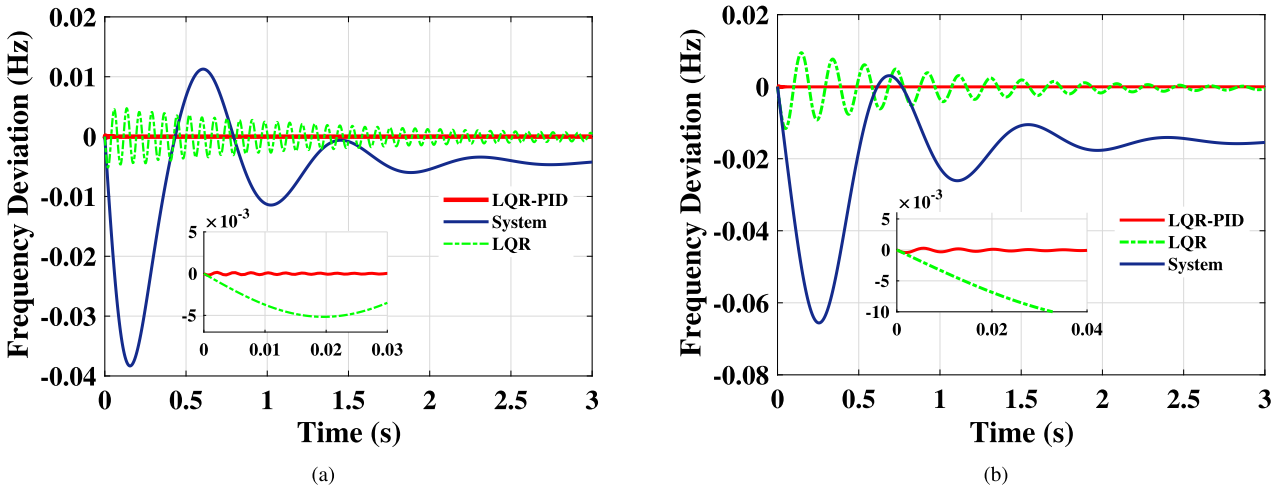

FIGURE 7. Considering a nominal load 0.05 pu for both areas: (a) Frequency deviation of Area 1, (b) Frequency deviation of Area 2.

harmonic oscillation and cannot eliminate steady-state errors. It also requires a large settling time. The LMI LQR-PID eliminates steady-state errors and requires less settling time. The results show that the proposed controller can eliminate a large amount of frequency deviation in the SG.

B. PERFORMANCE ANALYSIS WITH A LARGE POPULATION OF PHEVS

This section evaluates the effectiveness of the proposed controller with a large number of PHEVs connected to the SG. Fig. 8(a) and (b) show the resulting frequency deviations. For Area 1, the number of PHEVs has increased from 500 to 800, which increases the overshoot from 0.039 Hz to 0.15 Hz. Similarly, the PHEVs in Area 2 increased from 100 to 300, which is responsible for introducing excess overshoot from 0.062 Hz to 0.207 Hz. The proposed control strategy reduces the overshoot to 0.003 Hz and 0.005 Hz for Areas 1 and 2, respectively.

C. PERFORMANCE ANALYSIS WITH LARGE LOAD CHANGE

Fig. 9(a) and (b) show the frequency deviations of Areas 1 and 2 of the interconnected SG. These results indicate that the conventional model has the largest frequency deviation. The closed-loop response with the LQR controller reduces the frequency deviation, although it contains harmonic oscillation, cannot eliminate steady-state errors and requires a large settling time. The LMI LQR-PID eliminates steady-errors and requires less settling time. Hence, the proposed controller can eliminate a large amount of frequency deviation in the SG.

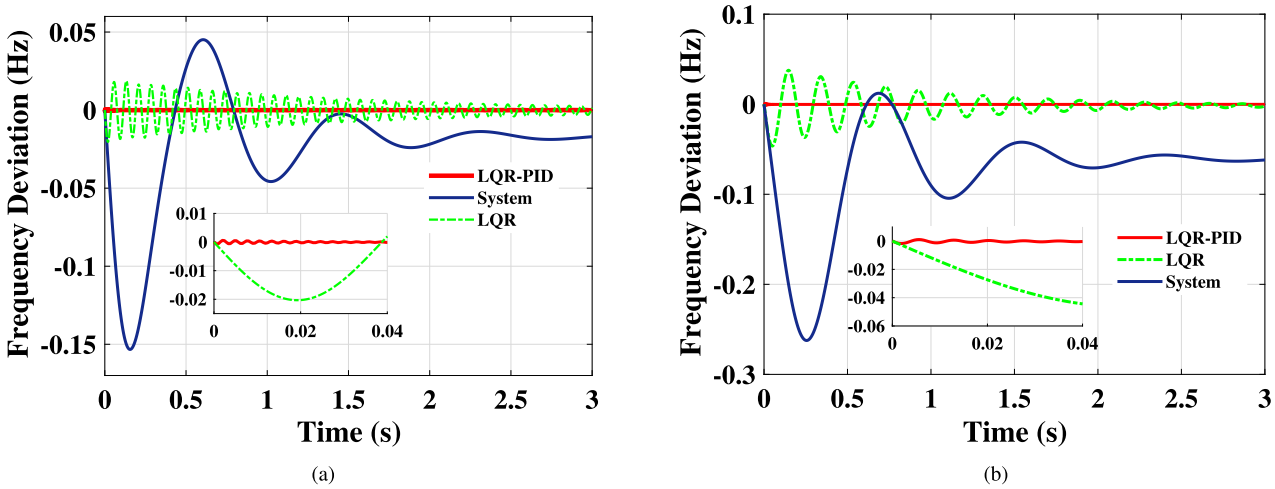

FIGURE 8. Impacts of a large population of PHEVs on frequency deviations in (a) Area 1 and (b) Area 2.

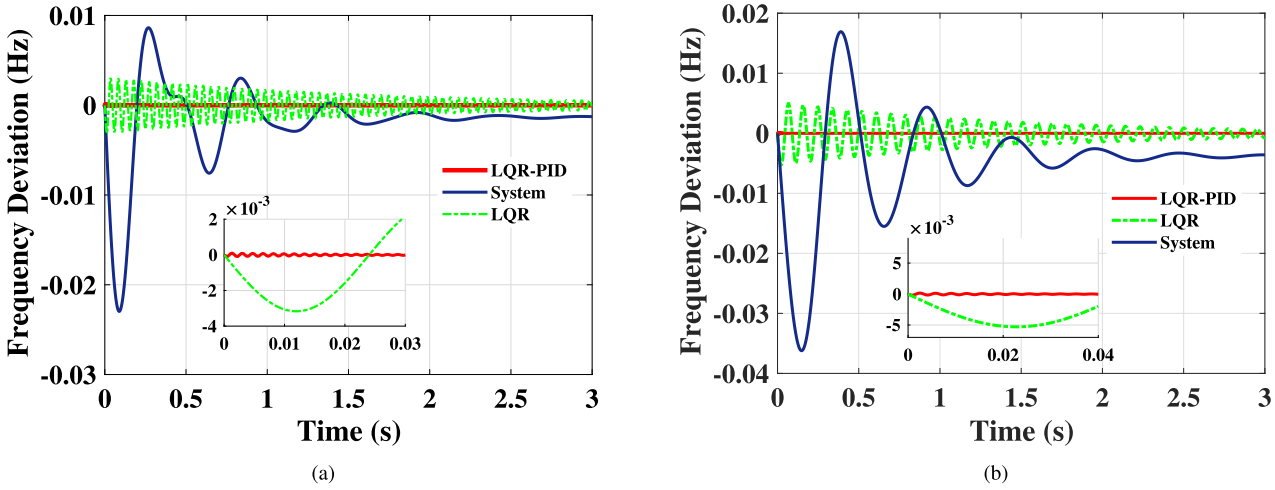

FIGURE 9. Impacts of a step load increase from 0.05 pu to 0.2 pu: Frequency deviations in (a) Area 1 and (b) Area 2.

D. PERFORMANCE ANALYSIS OF WIND POWER FLUCTUATION

The robustness of the proposed controller is now investigated with the presence of a renewable energy source (wind energy) in the SG. Fig. 10(a) and (b) show the frequency variations in Areas 1 and 2 in the presence of wind energy. Fig. 11 shows the wind power output. The open loop system model without any control technique provides undesirable frequency deviation. The adjusted model with the LQR controller improves the problem, although it is not in a nominal range. The proposed controller performs successful frequency compensation in the presence of wind energy.

E. PERFORMANCE ANALYSIS WITH TIE-LINE POWER DEVIATION

Fig. 12 presents the tie-line power deviation between Areas 1 and 2. The open loop response shows large power variation, which is undesirable. The LQR controller can improve the problem although there are unwanted oscillation and steady-state errors. The LMI LQR-PID controller can solve these problems effectively. The results show that the proposed controller keeps frequency deviations within an acceptable range.

TABLE 2. Comparison of closed-loop performances.

Response Characteristics	LMI LQR-PID Controller	LQR Controller
Rising Time $(T_r)(sec)$	0.0272	0.916
Settling Time $(T_s)(sec)$	0.0506	2.22
Percent Overshoot	0	2.53

TABLE 3. Comparisons of advantages between the controllers.

Name of the controller	Advantages	Limitations
LMI LQR-PID Controller	(i) High band width, (ii) Large gain and phase margin, (iii) Robust, (iV) Tracks reference signal	-
LQR Controller [59]	(i) High band width,	(i) Does not track reference signal, (ii) Low operating region
LQG Controller [60]	(i) High band width,	(i) Does not track reference signal
Model Predictive Controller [61]	(i) Large gain and phase margin, (ii) Robust, (iii) Low noise	(i) Low band-width
H_∞ Controller [47]	(i) Deal with uncertainties and disturbance, (ii) Small harmonic distortion, (iii) Easy to implement	(i) Higher order (ii) Computational burden

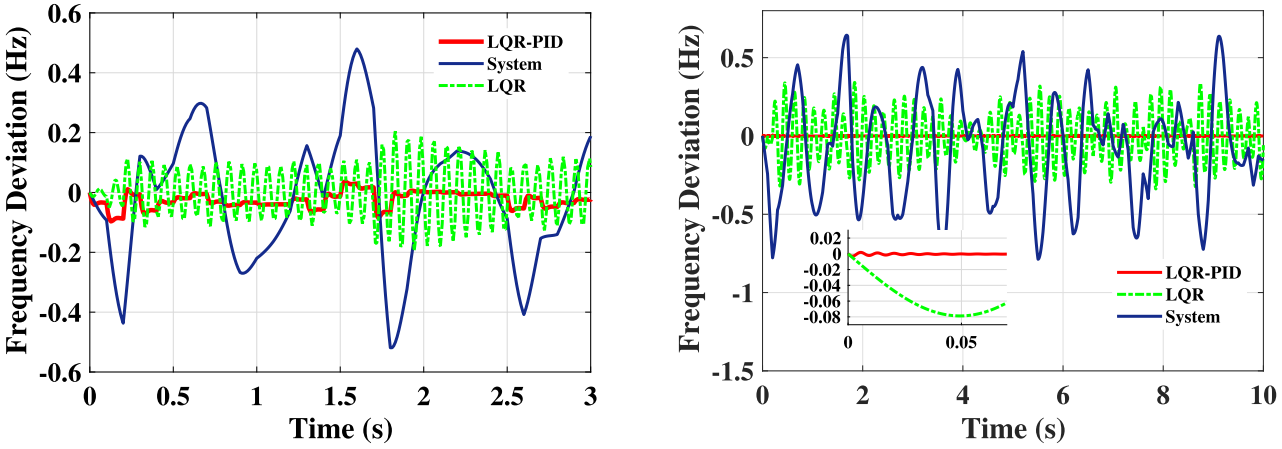

FIGURE 10. Effect of wind power: Frequency deviations in (a) Area 1 (b) Area 2.

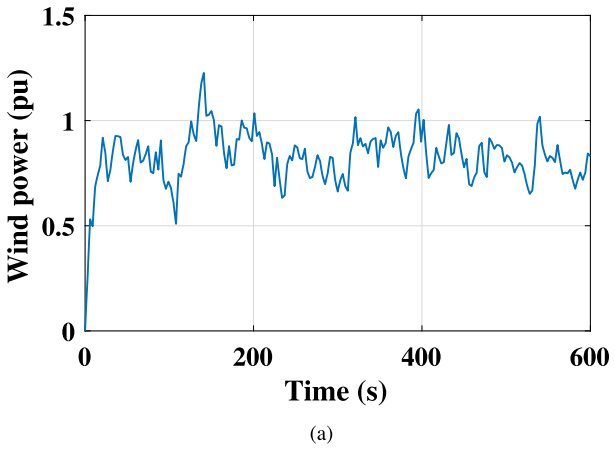

FIGURE 11. Wind power output.

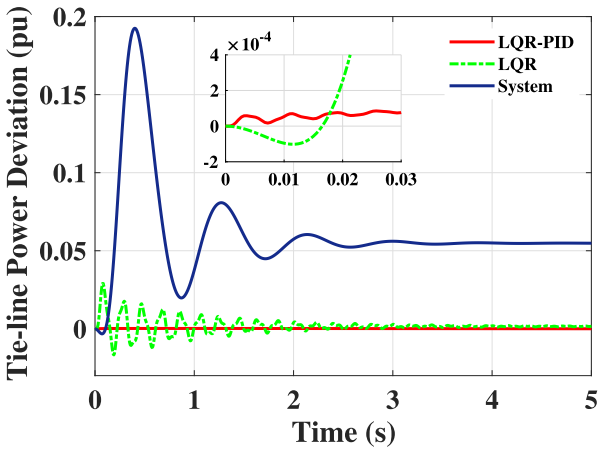

FIGURE 12. Tie-line power deviation.

F. COMPARATIVE STUDY OF THE PERFORMANCE OF THE CONTROLLERS

A comparison of the performance using the proposed controller and the standard linear quadratic regulator in terms of rise time, settling time, and percentage overshoot is presented in Table 2. The comparison shows that the proposed controller requires less settling and rising time as compared to the LQR controller. Although the LQR controller shows smaller overshoot as compared to the proposed controller but the LQR controller is unable to track the reference signal. Importantly, the LQR controller has lower bandwidth in comparison with the proposed controller as shown Fig. 6(b). The advantages of the proposed controller as compared to the some of the existing controllers available in the literature are shown in Table 3. The comparison shows that the proposed controller provides high performance as compared to the other controllers.

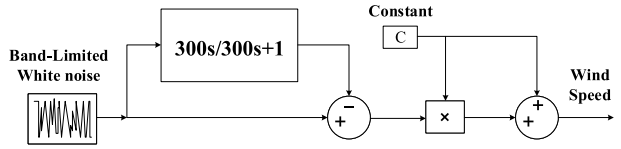

FIGURE 13. Wind speed model.

V. CONCLUSION

An LQR-PID controller was developed in this paper for frequency stabilization of a two-area interconnected SG system. The controller was designed based on the linear matrix inequality approach. A comparative study was made to determine the optimum frequency stabilization for the system. The simulation and comparative study results demonstrate the superior robustness of the LQR-PID controller. The proposed controller provides high gain, high bandwidth, and robust performance. The results of this paper provide a method of optimal frequency stabilization for a two-area interconnected SG. The results demonstrate that the LQR-PID controller is able to achieve a fast transient response for frequency stabilization in a two-area interconnected system.

APPENDIX

The modeling of wind speed [61] is presented in Fig. 13. The wind speed was defined by multiplying an arbitrary fluctuation derived from the noise block associated with the low pass filter in Matlab/Simulink to assess arbitrary wind speed variation.

REFERENCES

[1] H. Bevrani, A. Ghosh, and G. Ledwich, "Renewable energy sources and frequency regulation: Survey and new perspectives," *IET Renew. Power Gener.*, vol. 4, no. 5, pp. 438–457, Sep. 2010.

[2] M. S. Hossain, N. A. Madlool, N. A. Rahim, J. Selvara, A. K. Pandey, and A. F. Khan, "Role of smart grid in renewable energy: An overview," *Renew. Sustain. Energy Rev.*, vol. 60, pp. 1168–1184, Jul. 2016.

[3] M. Dreidy, H. Mokhlis, and S. Mekhilef, "Inertia response and frequency control techniques for renewable energy sources: A review," *Renew. Sustain. Energy Rev.*, vol. 69, pp. 144–155, Mar. 2017.

[4] X. Fang, S. Misra, G. Xue, and D. Yang, "Smart grid—The new and improved power grid: A survey," *IEEE Commun. Surveys Tuts.*, vol. 14, no. 4, pp. 944–980, 4th Quart., 2012.

[5] O. Rahbari, M. Vafaeipour, N. Omar, M. A. Rosen, O. Hegazy, J.-M. Timmermans, S. Heibati, and P. van den Bossche, "An optimal versatile control approach for plug-in electric vehicles to integrate renewable energy sources and smart grids," *Energy*, vol. 134, pp. 1053–1067, Sep. 2017.

[6] C. Peng, J. Zou, and L. Lian, "Dispatching strategies of electric vehicles participating in frequency regulation on power grid: A review," *Renew. Sustain. Energy Rev.*, vol. 68, pp. 147–152, Feb. 2017.

[7] E. Tian, Z. Wang, L. Zou, and D. Yue, "Chance-constrained H_∞ control for a class of time-varying systems with stochastic nonlinearities: The finite-horizon case," *Automatica*, vol. 107, pp. 296–305, Sep. 2019.

[8] H. H. Alhelou, M.-E. Hamedani-Golshan, R. Zamani, E. Heydarian-Forushani, and P. Siano, "Challenges and opportunities of load frequency control in conventional, modern and future smart power systems: A comprehensive review," *Energies*, vol. 11, no. 10, p. 2497, 2018.

[9] H. H. Alhelou, M. E. Hamedani-Golshan, T. C. Njenda, and P. Siano, "A survey on power system blackout and cascading events: Research motivations and challenges," *Energies*, vol. 12, no. 4, p. 628, 2019.

[10] S. Falahati, S. A. Taher, and M. Shahidehpour, "A new smart charging method for EVs for frequency control of smart grid," *Int. J. Elect. Power Energy Syst.*, vol. 83, pp. 458–469, Dec. 2016.

[11] K. M. Tan, V. K. Ramachandaramurthy, and J. Y. Yong, "Integration of electric vehicles in smart grid: A review on vehicle to grid technologies and optimization techniques," *Renew. Sustain. Energy Rev.*, vol. 53, pp. 720–732, Jan. 2016.

[12] C. M. Martinez, X. Hu, D. Cao, E. Velenis, B. Gao, and M. Wellers, "Energy management in plug-in hybrid electric vehicles: Recent progress and a connected vehicles perspective," *IEEE Trans. Veh. Technol.*, vol. 66, no. 6, pp. 4534–4549, Jun. 2017.

[13] T. Masuta and A. Yokoyama, "Supplementary load frequency control by use of a number of both electric vehicles and heat pump water heaters," *IEEE Trans. Smart Grid*, vol. 3, no. 3, pp. 1253–1262, Sep. 2012.

[14] M. Yilmaz and P. T. Krein, "Review of the impact of vehicle-to-grid technologies on distribution systems and utility interfaces," *IEEE Trans. Power Electron.*, vol. 28, no. 12, pp. 5673–5689, Dec. 2013.

[15] J. Pahasa and I. Ngamroo, "Coordinated control of wind turbine blade pitch angle and PHEVs using MPCs for load frequency control of microgrid," *IEEE Syst. J.*, vol. 10, no. 1, pp. 97–105, Mar. 2016.

[16] M. Takagi, H. Yamamoto, K. Yamaji, K. Okano, R. Hiwatari, and T. Ikeya, "Load frequency control method by charge control for plug-in hybrid electric vehicles with LFC signal," *IEEJ Trans. Power Energy*, vol. 129, no. 11, pp. 1342–1348, Jan. 2009.

[17] V. C. Gungor, D. Sahin, T. Kocak, S. Ergut, C. Buccella, C. Cecati, and G. P. Hancke, "A survey on smart grid potential applications and communication requirements," *IEEE Trans. Ind. Informat.*, vol. 9, no. 1, pp. 28–42, Feb. 2013.

[18] R. Sagotra, "Frequency regulation of interconnected power system with the introduction of communication delay in smart grid," Ph.D. dissertation, Thapar Inst. Eng. Technol., Patiala, India, 2018.

[19] A. Mohanty, M. Viswavandya, P. K. Ray, and S. Patra, "Stability analysis and reactive power compensation issue in a microgrid with a DFIG based WECS," *Int. J. Elect. Power Energy Syst.*, vol. 62, pp. 753–762, Nov. 2014.

[20] K. Chatterjee, "Design of dual mode PI controller for load frequency control," *Int. J. Emerg. Electr. Power Syst.*, vol. 11, no. 4, pp. 1–24, 2011.

[21] H. Bevrani and T. Hiyama, "On load–frequency regulation with time delays: Design and real-time implementation," *IEEE Trans. Energy Convers.*, vol. 24, no. 1, pp. 292–300, Mar. 2009.

[22] T. H. Mohamed, H. Bevrani, A. A. Hassan, and T. Hiyama, "Decentralized model predictive based load frequency control in an interconnected power system," *Energy Convers. Manage.*, vol. 52, no. 2, pp. 1208–1214, 2011.

[23] J. Nanda, S. Mishra, P. G. Mishra, and K. V. Sajith, "A novel classical controller for automatic generation control in thermal and hydrothermal systems," in *Proc. Joint Int. Conf. Power Electron., Drives Energy Syst. (PEDES) Power India*, Dec. 2010, pp. 1–6.

[24] A. Yazdizadeh, M. H. Ramezani, and E. Hamedrahmat, "Decentralized load frequency control using a new robust optimal MISO PID controller," *Int. J. Elect. Power Energy Syst.*, vol. 35, no. 1, pp. 57–65, 2012.

[25] L. C. Saikia, A. Bharali, O. Dixit, T. Malakar, B. Sharma, and S. Kouli, "Automatic generation control of multi-area hydro system using classical controllers," in *Proc. 1st Int. Conf. Power Energy NERIST (ICPEN)*, Dec. 2012, pp. 1–6.

[26] H. S. Ko and J. Jatskevich, "Power quality control of wind-hybrid power generation system using fuzzy-LQR controller," *IEEE Trans. Energy Convers.*, vol. 22, no. 2, pp. 516–527, Jun. 2007.

[27] S. H. Shahalami and D. Farsi, "Analysis of load frequency control in a restructured multi-area power system with the Kalman filter and the LQR controller," *AEU-Int. J. Electron. Commun.*, vol. 86, pp. 25–46, Mar. 2018.

[28] H. Liu, Z. Hu, Y. Song, and J. Lin, "Decentralized vehicle-to-grid control for primary frequency regulation considering charging demands," *IEEE Trans. Power Syst.*, vol. 28, no. 3, pp. 3480–3489, Aug. 2013.

[29] K. Yamashita and H. Miyagi, "Multivariable self-tuning regulator for load frequency control system with interaction of voltage on load demand," *IEE Proc. D—Control Theory Appl.*, vol. 138, no. 2, pp. 177–183, Mar. 1991.

[30] C. T. Pan and C. M. Liaw, "An adaptive controller for power system load-frequency control," *IEEE Trans. Power Syst.*, vol. 4, no. 1, pp. 122–128, Feb. 1989.

[31] C. S. Rao, "Adaptive neuro fuzzy based load frequency control of multi area system under open market scenario," in *Proc. Int. Conf. Adv. Eng., Sci. Manage. (ICAESM)*, Mar. 2012, pp. 5–10.

[32] M. Masiala, M. Ghribi, and A. Kaddouri, "An adaptive fuzzy controller gain scheduling for power system load-frequency control," in *Proc. IEEE Int. Conf. Ind. Technol. (ICIT)*, vol. 3, Dec. 2004, pp. 1515–1520.

[33] G. Ray, A. N. Prasad, and G. D. Prasad, "A new approach to the design of robust load-frequency controller for large scale power systems," *Electr. Power Syst. Res.*, vol. 51, no. 1, pp. 13–22, 1999.

[34] I. R. Fitri, J.-S. Kim, and H. Song, "High-gain disturbance observer-based robust load frequency control of power systems with multiple areas," *Energies*, vol. 10, no. 5, p. 595, 2017.
[35] Y. Wang, R. Zhou, and C. Wen, "New robust adaptive load-frequency control with system parametric uncertainties," *IEE Proc.-Gener., Transmiss. Distrib.*, vol. 141, no. 3, pp. 184–190, May 1994.
[36] H. Bevrani, "Robust load frequency controller in a deregulated environment: A mu-synthesis approach," in *Proc. IEEE Int. Conf. Control Appl.*, vol. 1, Aug. 1999, pp. 616–621.
[37] H. Shayeghi and H. Shayanfar, "Application of ANN technique for interconnected power system load frequency control," *IJE Trans. B, Appl.*, vol. 16, no. 3, Oct. 2003.
[38] M. Datta and T. Senjyu, "Fuzzy control of distributed PV inverters/energy storage systems/electric vehicles for frequency regulation in a large power system," *IEEE Trans. Smart Grid*, vol. 4, no. 1, pp. 479–488, Mar. 2013.
[39] C. Chang and W. Fu, "Area load frequency control using fuzzy gain scheduling of pi controllers," *Electr. Power Syst. Res.*, vol. 42, no. 2, pp. 145–152, 1997.
[40] C. Chang, W. Fu, and F. Wen, "Load frequency control using genetic-algorithm based fuzzy gain scheduling of PI controllers," *Electr. Mach. Power Syst.*, vol. 26, no. 1, pp. 39–52, 1998.
[41] S. K. Pandey, S. R. Mohanty, and N. Kishor, "A literature survey on load–frequency control for conventional and distribution generation power systems," *Renew. Sustain. Energy Rev.*, vol. 25, pp. 318–334, Sep. 2013.
[42] C. Lee and S. M. Salapaka, "Fast robust nanopositioning—A linear-matrix-inequalities-based optimal control approach," *IEEE/ASME Trans. Mechatronics*, vol. 14, no. 4, pp. 414–422, Aug. 2009.
[43] A. Chatterjee, R. Chatterjee, F. Matsuno, and T. Endo, "Augmented stable fuzzy control for flexible robotic arm using LMI approach and neuro-fuzzy state space modeling," *IEEE Trans. Ind. Electron.*, vol. 55, no. 3, pp. 1256–1270, Mar. 2008.
[44] F. Liao, J. L. Wang, and G.-H. Yang, "Reliable robust flight tracking control: An LMI approach," *IEEE Trans. Control Syst. Technol.*, vol. 10, no. 1, pp. 76–89, Jan. 2002.
[45] G. Rizzello, D. Naso, B. Turchiano, and S. Seelecke, "Robust position control of dielectric elastomer actuators based on LMI optimization," *IEEE Trans. Control Syst. Technol.*, vol. 24, no. 6, pp. 1909–1921, Feb. 2016.
[46] R. Conway, J. Choi, R. Nagamune, and R. Horowitz, "Robust track-following controller design in hard disk drives based on parameter dependent Lyapunov functions," *IEEE Trans. Magn.*, vol. 46, no. 4, pp. 1060–1068, Apr. 2010.
[47] T. N. Pham, H. Trinh, and L. Van Hien, "Load frequency control of power systems with electric vehicles and diverse transmission links using distributed functional observers," *IEEE Trans. Smart Grid*, vol. 7, no. 1, pp. 238–252, Jan. 2016.
[48] K. Janfeshan and M. A. Masoum, "Hierarchical supervisory control system for PEVs participating in frequency regulation of smart grids," *IEEE Power Energy Technol. Syst. J.*, vol. 4, no. 4, pp. 84–93, Sep. 2017.
[49] S. Vachirasricirikul and I. Ngamroo, "Robust controller design of heat pump and plug-in hybrid electric vehicle for frequency control in a smart microgrid based on specified-structure mixed H_2/H_∞ control technique," *Appl. Energy*, vol. 88, no. 11, pp. 3860–3868, 2011.
[50] I. Ngamroo, "Specified structure mixed H_2/H_∞ control-based robust frequency stabilization in a smart grid by plug-in hybrid electric vehicles," *Int. J. Innov. Comput., Inf. Control*, vol. 9, no. 1, pp. 81–97, 2013.
[51] Y. Ota, H. Taniguchi, T. Nakajima, K. M. Liyanage, J. Baba, and A. Yokoyama, "Autonomous distributed V2G (vehicle-to-grid) satisfying scheduled charging," *IEEE Trans. Smart Grid*, vol. 3, no. 1, pp. 559–564, Mar. 2012.
[52] H. Yang, C. Y. Chung, and J. Zhao, "Application of plug-in electric vehicles to frequency regulation based on distributed signal acquisition via limited communication," *IEEE Trans. Power Syst.*, vol. 28, no. 2, pp. 1017–1026, May 2013.
[53] S. Vachirasricirikul and I. Ngamroo, "Robust LFC in a smart grid with wind power penetration by coordinated V2G control and frequency controller," *IEEE Trans. Smart Grid*, vol. 5, no. 1, pp. 371–380, Jan. 2014.
[54] M. Ge, M.-S. Chiu, and Q.-G. Wang, "Robust PID controller design via LMI approach," *J. Process Control*, vol. 12, no. 1, pp. 3–13, 2002.
[55] J. G. Van Antwerp and R. D. Braatz, "A tutorial on linear and bilinear matrix inequalities," *J. Process Control*, vol. 10, no. 4, pp. 363–385, 2000.
[56] J. Willems, "Least squares stationary optimal control and the algebraic Riccati equation," *IEEE Trans. Autom. Control*, vol. 16, no. 6, pp. 621–634, Dec. 1971.
[57] M. Armin, P. N. Roy, S. K. Sarkar, and S. K. Das, "LMI-based robust PID controller design for voltage control of islanded microgrid," *Asian J. Control*, vol. 20, no. 5, pp. 2014–2025, 2018.
[58] K. Liao and Y. Xu, "A robust load frequency control scheme for power systems based on second-order sliding mode and extended disturbance observer," *IEEE Trans. Ind. Informat.*, vol. 14, no. 7, pp. 3076–3086, Jul. 2018.
[59] M. Rahman, S. K. Sarkar, S. K. Das, and Y. Miao, "A comparative study of LQR, LQG, and integral LQG controller for frequency control of interconnected smart grid," in *Proc. 3rd Int. Conf. Elect. Inf. Commun. Technol. (EICT)*, Dec. 2017, pp. 1–6.
[60] M. Elsisi, M. Soliman, M. A. S. Aboelela, and W. Mansour, "Model predictive control of plug-in hybrid electric vehicles for frequency regulation in a smart grid," *IET Gener., Transmiss. Distrib.*, vol. 11, no. 16, pp. 3974–3983, 2017.
[61] X. Li, D. Hui, X. Lai, and T. Yan, "Power quality control in wind/fuel cell/battery/hydrogen electrolyzer hybrid micro-grid power system," in *Applications and Experiences of Quality Control*. Rijeka, Croatia: InTechOpen, 2011.

SAJAL KUMAR DAS received the Ph.D. degree in electrical engineering from the University of New South Wales, Australia, in 2014. In May 2014, he was appointed as a Research Engineer with the National University of Singapore (NUS), Singapore. In January 2015, he joined with the Department of Electrical and Electronic Engineering, American International University-Bangladesh (AIUB), as an Assistant Professor. He continued his work at AIUB, until he joined with the Department of Mechatronics Engineering, Rajshahi University of Engineering & Technology (RUET), as a Lecturer, in September 2015, where he is currently an Assistant Professor. His research interests include control theory and applications, mechatronics system control, robotics, and power system control.

MIZANUR RAHMAN was born in Bangladesh, in 1996. He received the B.Sc. degree in mechatronics engineering from the Rajshahi University of Engineering & Technology (RUET), Rajshahi, Bangladesh. He is also an Active Reviewer of many reputed journals. His research interests include control theory and applications, robust control of smart grid, and microgrid.

SANJOY KUMAR PAUL received the Ph.D. degree from the University of New South Wales.

He is currently with the UTS Business School, University of Technology Sydney, Australia. He has several years of experience as an academician. He has published more than 50 articles in top-tier journals and conferences, including *European Journal of Operational Research*, *International Journal of Production Economics*, *Computers & Operations Research*, *International Journal of Production Research*, *Annals of Operations Research*, *Journal of Management in Engineering*, *Journal of Cleaner Production, Computers and Industrial Engineering*, *Journal of Retailing and Consumer Services*, and *Journal of Intelligent Manufacturing*. He is also an Active Reviewer of many reputed journals. His research interests include supply chain risk management, modeling, applied operations research, and intelligent decision making. He is a member of the Australian Society for Operations Research (ASOR) and Australasian Supply Chain Institute (ASCI). He is also a Committee Member of the Industry Risk Committee of ASCI. He has received several awards in his career, including ASOR Rising Star Award, Excellence in Early Career Research Award from the UTS Business School, the Stephen Fester prize for most outstanding thesis from UNSW, and High Impact Publications Award for publishing articles in top-tier journals. He is a Guest Editor, an Associate Editor, and an Editorial Board Member of several journals.

MANIZA ARMIN was born in Dhaka, Bangladesh. She received the B.Sc. degree in mechatronics engineering from the Rajshahi University of Engineering & Technology (RUET), Rajshahi, Bangladesh. She is currently involved in robust control of both smart grid and microgrid. Her research interests include control applications, power system control, the IoT, and robotics.

PRIYO NATH ROY was born in Bangladesh. He received the B.Sc. degree in mechatronics engineering from the Rajshahi University of Engineering & Technology (RUET), Rajshahi, Bangladesh. In July 2019, he joined with the Department of Mechatronics Engineering, Khulna University of Engineering & Technology, as a Lecturer. He is currently involved in robust control of both smart grid and microgrid. His research interests include control applications, power system control, the IoT, and robotics.

NOROTTOM PAUL received the degree from the Rajshahi University of Engineering & Technology (RUET). He is currently pursuing the M.Sc. degree with the Bangladesh University of Engineering & Technology (BUET), where he involved in research on technology management. He is also an Engineer with Bangladesh Hi-Tech Park Authority (BHTPA) under Information and Communication Division, Bangladesh.